James K. Feathers &
Daniel A. Bush
Department of Anthropology, University of Washington, Box 353100, Seattle, WA, 98195-3100, U.S.A. E-mail: jimf@u.washington.edu guans@u.washington.edu

Received 18 May 1998
Revision received 22 March 1999 and accepted 7 June 1999

Keywords: luminescence dating, Die Kelders, Middle Stone Age, aeolian sediments, South Africa.

Luminescence dating of Middle Stone Age Deposits at Die Kelders

Luminescence dating of sediments has not been used extensively for dating Middle Stone Age deposits in South Africa, despite its potential for contributing to a poorly dated record. Such deposits at Die Kelders cave, on the southern South African coast, consist of narrow bands of occupation debris separated by thicker layers of aeolian sands containing much less evidence of occupation. Homogeneous, aeolian sediments are usually considered ideal for luminescence dating. Here we report luminescence analyses of five samples from these sands that demonstrate sufficient bleaching prior to burial to validate dating and that yield ages of about 60–70 ka, in agreement with other evidence from sedimentology, archaeology and electron spin resonance. Lack of significant differences in the ages suggests the deposits accumulated fairly rapidly during the early part of the Last Glaciation.

Journal of Human Evolution (2000) **38,** 91–119
Article No. jhev.1999.0351
Available online at http://www.idealibrary.com on IDEAL®

Introduction

Dating Middle Stone Age (MSA) deposits in southern Africa has long been problematic because much of the MSA is older than the practical limits of radiocarbon. Reliance has necessarily been placed on less accepted techniques. Among these, luminescence dating of sediments seems a suitable choice. Its dating range encompasses the MSA and it can date directly any depositional events that can be associated with exposure to sufficient sunlight. Yet, luminescence has so far been sparingly used for the MSA (Brooks *et al.*, 1995; Feathers, 1997; Grün *et al.*, 1996). Part of the problem is that much of the known MSA record is contained in rockshelters and caves, complex sediment traps likely to provide less than ideal dating targets in terms of assessing radioactivity and of assuring sufficient bleaching in antiquity (e.g., Roberts *et al.*, 1998).

Die Kelders Cave, on the southern South African coast, seems exceptional in this regard. The MSA deposits consist of a series of thin ''occupation horizons'' rich in artefacts, macrofauna and organic material, separated by thicker ''non-occupation horizons'' of rather homogeneous quartzose sand (Avery *et al.*, 1997; Grine *et al.*, 1991; Marean *et al.*, this volume; Tankard & Schweitzer, 1974). The latter do contain some localized concentrations of bone and organic material but are largely free of occupational debris that could complicate radioactivity assessment. Moreover, the well-sorted sands of the non-occupation horizons are best interpreted from textural evidence as aeolian deposits, believed derived from ancient dunes on the now-submerged continental shelf (Tankard & Schweitzer, 1976). Homogeneous aeolian deposits are generally considered the best candidates for successful luminescence dating. Since the non-occupation layers neatly divide a series of more intense occupations, they provide an opportunity for a stratigraphic series of dates that bracket the occupational events of interest.

There are some possible complications. One is contamination by poorly bleached

0047–2484/00/010091+29$35.00/0

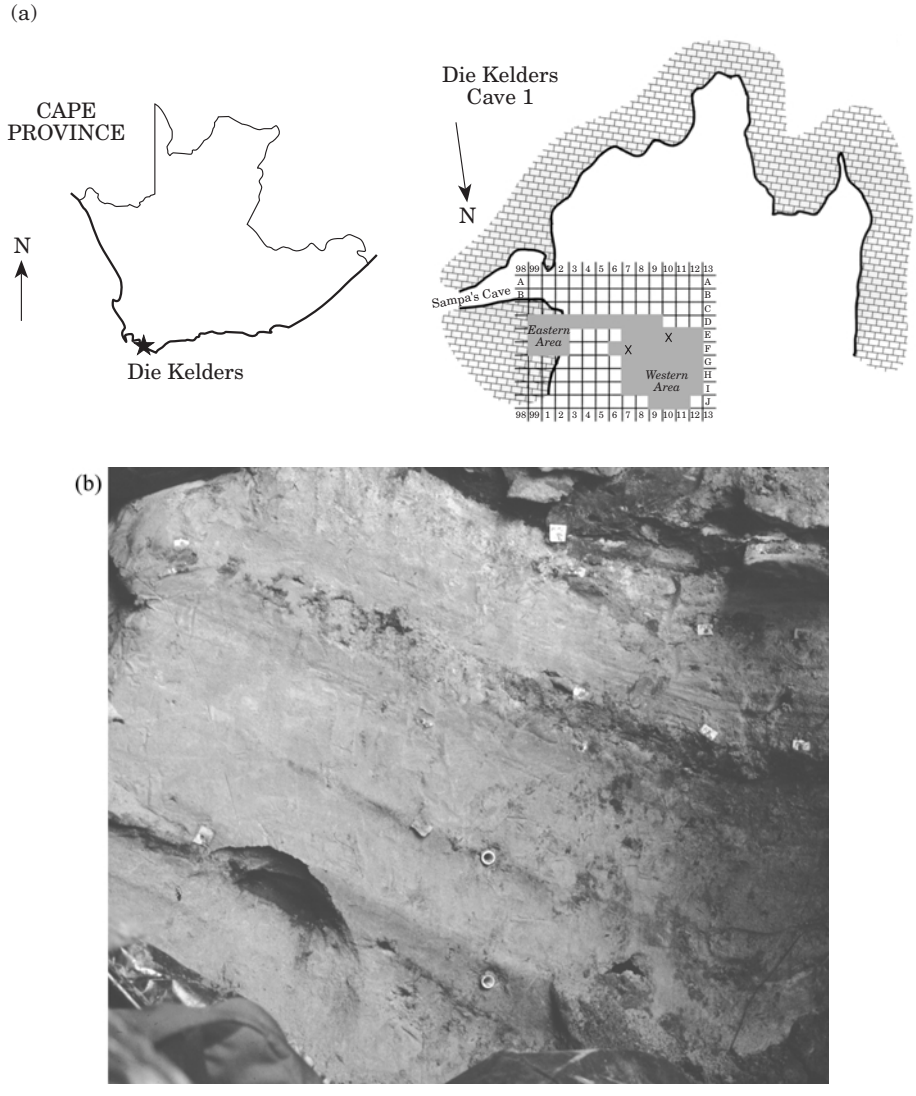

Figure 1. (a) and (b).

grains. The rockshelter formed at an unconformity between underlying quartzite and overlying limestone. Perched above the opening are calcined aeolianites. Limestone roof fall fragments in various stages of disintegration are found throughout the deposits. Quartz or feldspar grains entrapped in the limestone (Butzer, 1979) and subsequently freed during disintegration is one source of poorly bleached grains. Such grains could also be contributed by fragments of quartzite and aeolianite incorporated in some of the deposits (Goldberg, personal communication). Another complication is evidence of eluviation. Many sand grains exhibit pellicular coatings of clay or organic material on the upper surfaces (Avery *et al.*, 1997). Translocation, particularly of clay, might alter the natural radioactivity of the layers through time.

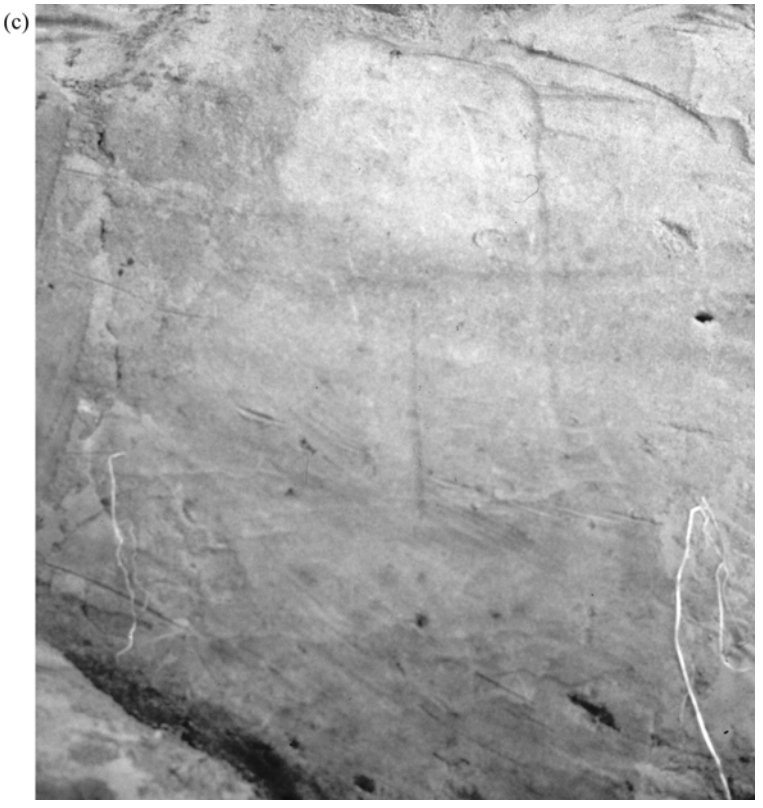

Figure 1. (c).

Figure 1. Location of the luminescence samples. (a) Map showing the excavation units within Cave 1. Sample locations are marked with an ''X''. The samples from Layers 7, 9, 11, and 13 were drawn from the south face of excavation square F7. The samples from Layer 4/5 were drawn from the south face of excavation square E10. (b) Photo of the F7 profile, showing relatively sterile strata separated by dark, thin layers of occupational debris. Samples were taken from midpoints of the sterile strata, from top to bottom, Layers 7, 9, 11 and 13. (c) Photo of the E10 profile showing the massive Layer 4/5. The circle near the top of the photo is the end of the sample collection tube. (Photos by Barbara S. Hay.)

Samples and procedures

Four samples were collected in a stratigraphic column in the eastern part of the excavation from midpoints of layers 7, 9, 11 and 13, youngest to oldest, separating MSA occupation layers 6, 8, 10, and 12 (numbering after Tankard & Schweitzer, 1974). A fifth sample was collected west of the others from the upper part of the Layer 4/5 complex (Avery *et al.*, 1997). Figure 1 shows the locations. The samples were collected by driving a metal pipe into cleaned profiles and capping both ends. Small samples from the intervening occupation layers were collected for additional radioactivity assay. Sample locations were chosen far from visible roof fall.

Because of its abundance, quartz was chosen as the material for dating. A 90–125 μm size fraction was prepared for luminescence analysis for all samples. In addition, a 4–11 μm multi-mineral fraction was prepared for the samples from Layer 11 and Layer 13. This not only provided an independent assessment of the equivalent

Table 1 Radioactivity data

Sample	Technique	K (wt%)	U (ppm)	Th (ppm)
Layer 4/5 upper	γ-spectrometry	0·17 ± 0·02	2·48 ± 0·10	3·28 ± 0·20
Layer 4/5 lower	α-counting		1·40 ± 0·10	2·40 ± 0·59
	Flame photometry	0·13 ± 0·01		
Layer 6	DNA		1·07 ± 0·15	
	α-counting		2·36 ± 0·16	4·48 ± 0·75
	Flame photometry	0·29 ± 0·01		
Layer 7	γ-spectrometry	0·12 ± 0·02	1·91 ± 0·10	3·85 ± 0·21
Layer 8	α-counting		6·80 ± 0·36	3·04 ± 0·92
	Flame photometry	0·12 ± 0·01		
Layer 9	γ-spectrometry	0·12 ± 0·02	2·21 ± 0·12	4·16 ± 0·25
Layer 10	DNA		2·38 ± 0·15	
	α-counting		1·73 ± 0·14	5·82 ± 0·97
	Flame photometry	0·15 ± 0·01		
Layer 11	γ-spectrometry	0·07 ± 0·02	2·41 ± 0·10	5·17 ± 0·20
	α-counting		2·08 ± 0·16	5·68 ± 0·96
	Flame photometry	0·10 ± 0·01		
Layer 12 (1)	DNA		1·82 ± 0·15	
	α-counting		2·76 ± 0·17	2·50 ± 0·66
	Flame photometry	0·30 ± 0·01		
Layer 12	DNA		1·85 ± 0·15	
	α-counting		4·95 ± 0·28	3·22 ± 0·84
	Flame photometry	0·34 ± 0·01		
Layer 13	γ-spectrometry	0·10 ± 0·02	2·41 ± 0·07	4·80 ± 0·21
	α-counting		2·18 ± 0·15	4·56 ± 0·77
	Flame photometry	0·11 ± 0·01		
Layer 14	DNA		3·84 ± 0·18	
	α-counting		4·25 ± 0·26	6·29 ± 1·02
	Flame photometry	0·17 ± 0·01		

Dated samples in italics. Layer 12 was sampled in two locations. Techniques include gamma spectrometry, thick source alpha counting, delayed neutron analysis and atomic emission (flame photometry). Gamma spectrometry values for U and Th are weighted averages of several lines.

dose, but also allowed evaluation of possible contamination from grains released from roof fall. These should have a different size distribution than the aeolian sand and therefore differentially affect the age from the two fractions. The 90–125 μm quartz fraction was isolated by sieving, treatment with HCl and H_2O_2, etching for 40 min with 48% HF, and density separation from minerals heavier than 2·66 specific gravity using sodium polytungstate. The fine-grained fraction was isolated by settling in acetone after treatments with HCl and H_2O_2.

Thermoluminescence (TL), optically stimulated luminescence (OSL) and infra-red stimulated luminescence (IRSL) were employed for derivation of equivalent dose (D_E). TL and OSL were measured from the 90–125 μm quartz grains, IRSL from the fine-grains, the latter signal originating from feldspars. For TL, grains were dispersed on A1 planchets and normalized by weight. For OSL, a monolayer of grains was secured on A1 discs by silicone spray. The fine grains for IRSL were settled onto A1 discs. Normalization for OSL and IRSL used 0·1 s shines. Normalization for TL used weight. TL measurements were from the so-called slowly bleaching peak (SBP), which was isolated by removing faster bleaching components by exposure to 550 nm light,

Table 2 Disequilibrium data

Sample	^{232}Th chain		^{238}U chain			
	^{228}Ac (keV:338, 911)	^{212}Pb (keV:239)	^{234}Th (keV:63)	^{226}Ra (keV:186)	^{214}Pb/^{214}Bi (keV:295, 352,609)	^{210}Pb (keV:46)
Layer 4/5	3·58 ± 0·23	3·19 ± 0·13	2·46 ± 0·64	2·51 ± 0·16	2·46 ± 0·14	2·38 ± 0·47
Layer 7	4·06 ± 0·22	3·70 ± 0·13	1·48 ± 0·58	2·01 ± 0·17	1·84 ± 0·13	2·38 ± 0·46
Layer 9	4·18 ± 0·39	4·41 ± 0·15	3·03 ± 0·85	2·32 ± 0·18	2·06 ± 0·17	2·36 ± 0·56
Layer 11	5·75 ± 0·23	4·89 ± 0·12	1·99 ± 0·60	2·48 ± 0·16	2·37 ± 0·13	2·71 ± 0·49
Layer 13	5·39 ± 0·24	4·68 ± 0·13	2·44 ± 0·44	2·50 ± 0·09	2·22 ± 0·13	2·12 ± 0·64

Values are in ppm for parent in equilibrium. Where more than one energy is used, a weighted average is computed. ^{212}Pb at keV:239 has some interference from a much smaller uranium line which was subtracted by deconvoluting the peak. ^{226}Ra at 186 has interference from the ^{235}U chain, but this does not affect the calculated activity for samples in equilibrium if an assumption of constant ^{235}U/^{238}U ratio among samples and the standard used for calibration is made.

Table 3 Dose rates (Gy/ka) assuming 15% moisture

Sample	alpha	beta	gamma	Cosmic	Total
Layer 4/5	0·042 ± 0·023	0·439 ± 0·029	0·420 ± 0·024	0·027 ± 0·006	0·928 ± 0·044
Layer 7	0·038 ± 0·020	0·357 ± 0·025	0·442 ± 0·025	0·026 ± 0·005	0·863 ± 0·041
Layer 9	0·043 ± 0·022	0·389 ± 0·027	0·464 ± 0·027	0·025 ± 0·005	0·921 ± 0·045
Layer 11 (90–125 μm)	0·049 ± 0·026	0·396 ± 0·027	0·470 ± 0·026	0·025 ± 0·005	0·940 ± 0·046
Layer 11 (4–11 μm)	0·453 ± 0·046	0·470 ± 0·030	0·470 ± 0·026	0·025 ± 0·005	1·417 ± 0·061
Layer 13 (90–125 μm)	0·048 ± 0·025	0·411 ± 0·026	0·499 ± 0·027	0·024 ± 0·005	0·982 ± 0·045
Layer 13 (4–11 μm)	0·441 ± 0·044	0·484 ± 0·030	0·499 ± 0·027	0·024 ± 0·005	1·448 ± 0·060

following previously described procedures (Franklin & Hornyak, 1990; Feathers, 1997). TL glow curves were obtained on a Littlemore glow oven in N_2 atmosphere at 1°C/s. Luminescence was collected by an EMI 9635Q photomultiplier through Corning 7-59 (blue) and Schott UG-11 (ultraviolet) filters. OSL was measured using a halogen lamp source filtered to allow only 500–540 nm light onto the sample and IRSL was measured using 880 nm light emitting diodes, both on a Daybreak 1100 automated system, using a 9235Q photomultiplier with two Hoya U340 (ultraviolet) filters for OSL and two Schott BG39 (green-blue) filters for IRSL (Bortolot, 1997). Optical measurements were made at 100°C to limit influence of low temperature traps. Irradiations were by a ^{90}Sr beta source, calibrated against ^{137}Cs gamma sources, and a ^{241}Am alpha source.

D_E was determined using combined additive dose and regeneration procedures. Regeneration followed exposures of 30 min for OSL and IRSL and up to 22 hours for TL from a solar simulator (Applied Physics Model 9500). The "Australian slide" technique (Huntley *et al.*, 1993*a*), which controls for some of the problems in using either additive dose or regeneration alone (Prescott & Robertson, 1997), was employed in all cases. Both multi- and single-aliquot methods were employed for OSL, the single aliquot procedure following Duller (1995) and using the luminescence correction method.

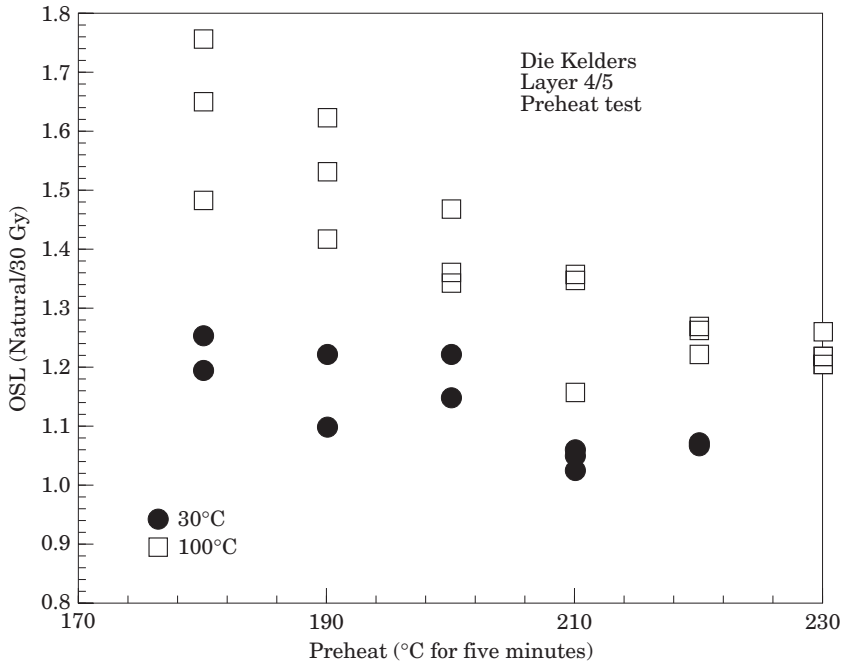

Figure 2. Ratio of the natural *vs.* regenerated (30 Gy) signal for several aliquots given different preheats for the sample from Layer 4/5. Data for OSL measured at 30°C and 100°C are shown. The ratios level out at higher preheats, indicating they have redistributed charge for the regeneration in a way comparable to that which occurred in nature.

Since the determination of D_E in OSL requires comparison of signals arising from both natural and laboratory irradiation, an elevated temperature ''preheat'' is required to make the signals comparable. The preheat serves to redistribute charge for the irradiated signal in such a way as to simulate the effects of storage for thousands of years at ambient temperatures for the natural signal (Smith & Rhodes, 1994; Wintle & Murray, 2000). To determine a proper preheat, the ratio of the natural signal and a regenerated signal (after 400 s exposure and 30 Gy irradiation) was calculated for 15 aliquots given preheats ranging from 180° to 220°C for 5 min. A plot of the ratios against preheat allows assessment of a plateau region satisfactory for dating (Murray *et al.*, 1997). Proper preheats so determined were then given to all natural and irradiated aliquots in subsequent analyses. The preheat test was originally performed measuring the OSL signal at 30°C; additional measurements were made at 100°C for three of the samples.

Natural/regenerated ratios can be used as well to assess adequate light exposure at time of deposition. The assumption is that poor bleaching will result in some grains being better bleached than others and that the poorly bleached grains will be differentially distributed from aliquot to aliquot. The ratios from many aliquots should be normally distributed and cover a narrow range for a homogeneous mix of well-bleached grains, but have a skewed distribution and wide range for poorly bleached sediments (Murray *et al.*, 1995; Lamothe & Auclair, 1997). The effect will be accentuated for aliquots containing only a few grains, although in the extreme case of single

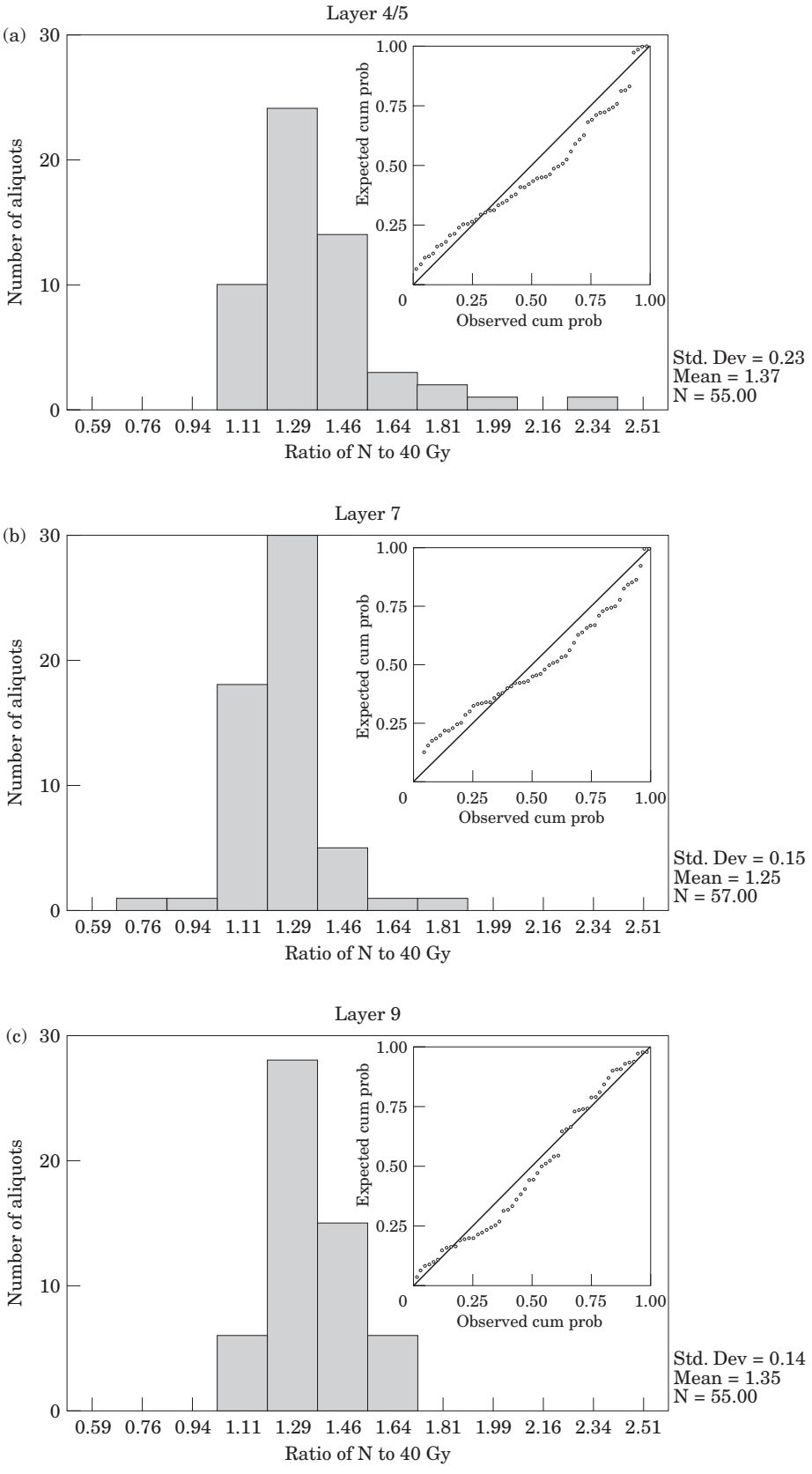

Figure 3. (a), (b) and (c).

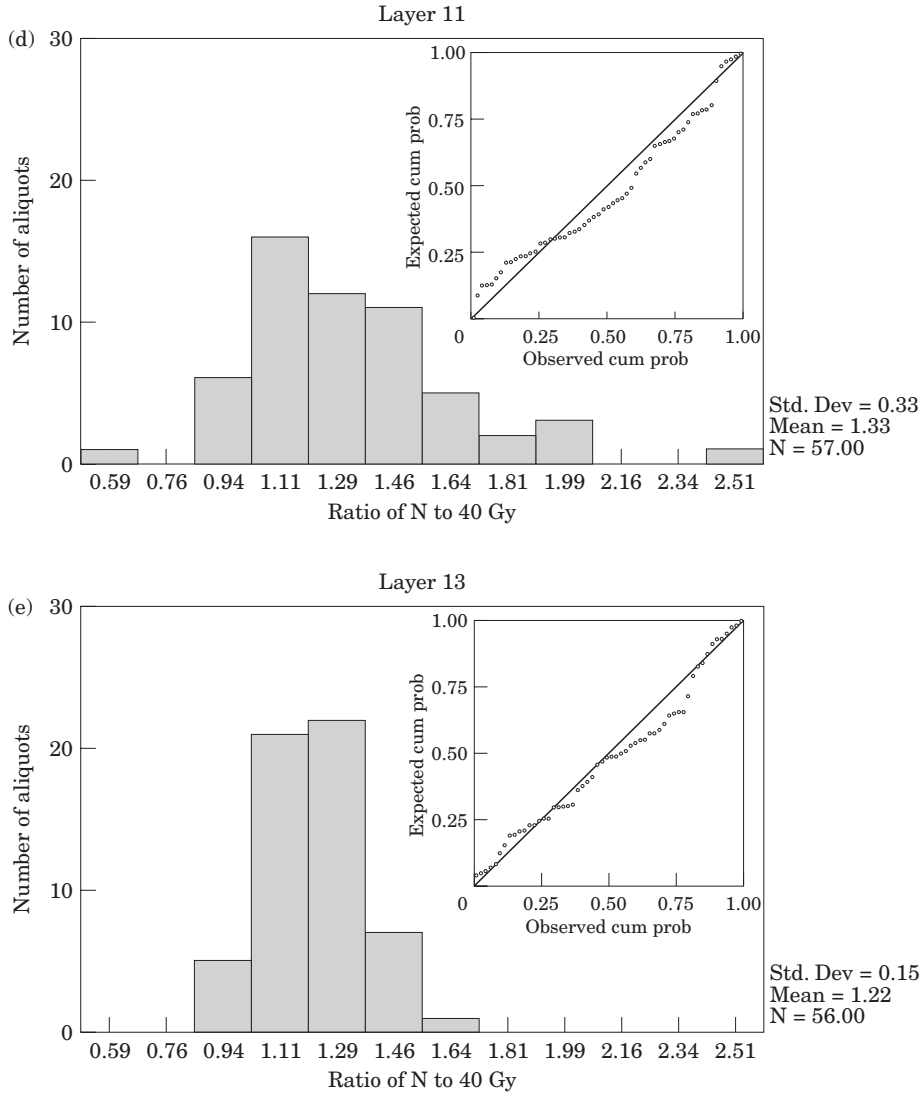

Figure 3. Histograms of ratios of natural *vs.* regenerated (40 Gy) signal, all given the same preheat, for each sample. The insets plot the cumulative probability of the observed data (dots) against the expected probability of a normal distribution (solid line). Significant deviation from normality, not apparent here, would suggest non-uniform bleaching of grains.

grains, heterogeneity in the radioactivity environment will broaden the distribution. For this analysis 57 aliquots of about 100 grains each were prepared for each sample. The natural and regenerated (after 400 s exposure and 40 Gy irradiation) signals were measured following a preheat as determined above. The possibility that all grains were poorly bleached, but uniformly so, can be tested by comparing components of the luminescence signal that bleach at different rates (for example, SBP versus OSL). Measuring the OSL of a modern surface sample, with a depositional history analogous to the

Table 4 Kolmogorov–Smirnov test for normality

Sample	K–S *z*-score	2-tailed *P*
Layer 4/5	0·9639	0·3107
Layer 7	0·8286	0·4984
Layer 9	0·7081	0·6978
Layer 11	0·8121	0·5246
Layer 13	1·2531	0·0865

ones of interest, is often recommended as a further test of proper zeroing. However, the stratigraphy at Die Kelders is capped by a Later Stone Age shell midden and thus provides no modern analog.

Radioactivity of the dated samples was measured by high resolution gamma spectrometry. The radioactivity of the intervening occupation layers was measured by thick-source alpha counting and delayed neutron analysis, the latter performed by the Saskatchewan Research Council. Two of the dated samples were also measured by thick-source alpha counting for comparison. Samples for thick-source alpha counting were milled to flour consistency. Evidence of disequilibrium in the decay chains and the distribution of radiaoctivity through the profile can provide information on possible movement of radionuclides through time. Moisture content was estimated from a sample collected in an air-tight bag, although current moisture contents are not likely to be representative of past conditions. This will be discussed further.

Dose rate

tj;3The radioactivity data are presented in Tables 1 and 2. The gamma spectrometry results (Table 2) show that for the dated samples no statistically significant disequilibrium in the ^{238}U chain is evident. Gamma spectrometry does not give as complete a picture for the ^{232}Th chain, due to lack of strong emissions at the very top of the chain, although disequilibrium among ^{232}Th, ^{228}Rad and ^{228}Ac is rare (Murray *et al.*, 1987). Comparing emissions associated with ^{228}Ac and ^{212}Pb show the lower part of the chain in all samples close to equilibrium. The largest differences are with Layer 11 and Layer 13. However, comparison of the weighted averages of gamma emissions with the results from alpha counting (Table 1) for these two samples suggests no significant disequilibrium, in either chain. For dose rate calculations, the weighted averages of the various gamma emissions were used (Table 1).

Comparison of alpha counts with ^{238}U concentrations, determined from delayed neutron analysis, for the samples collected from the occupation layers reveals that the U-series in these are not in equilibrium, the parent being depleted in most cases. This may reflect the presence of abundant bone in these layers. The overall radioactive composition of these layers, however, is not significantly different than that of the non-occupation layers. Nor does there appear to be any general trend vertically in the profile that might suggest movement of radionuclides. This, coupled with the evidence of only localized disequilibrium, argues for long-term stability in the overall radioactive environment. The current dose rate is therefore likely to be representative of the dose rate since deposition. Dose rates (Table 3) were calculated following Nambi & Aitken (1986) giving allowance for beta and alpha attenuations (Aitken, 1985). The gamma dose rates were calculated using gradients based on the nearness of the non-occupation layers to the sample locations (after Aitken, 1985, appendix H).

The cosmic dose rate is strongly influenced by the configuration of the cave as well as the burial depth (2–3 m) of the samples. The full cosmic flux impinges on the surface of the cave through the cave opening, but from other directions it is attenuated by the thickness of the rock (about 5·5 m to the surface of the coastal

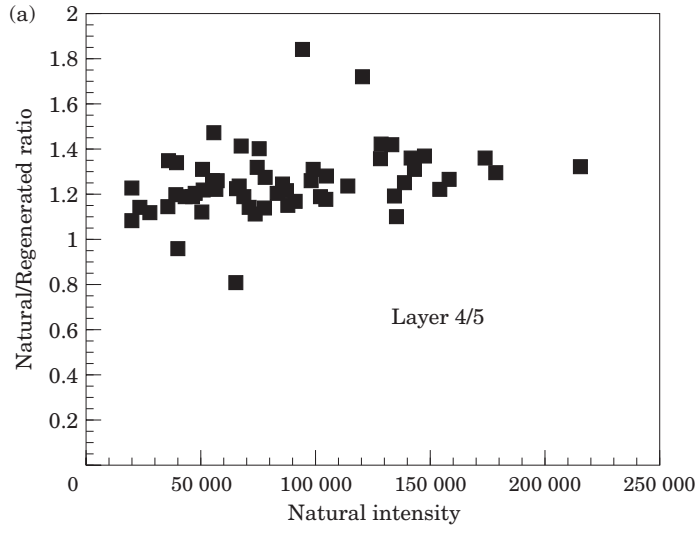

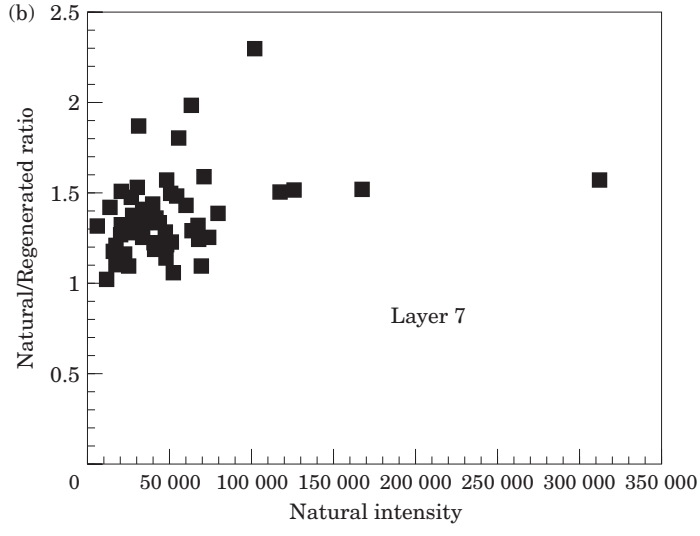

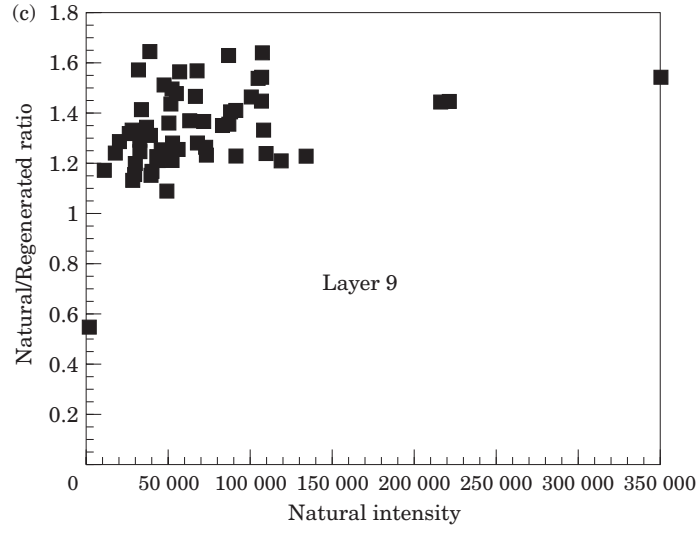

Figure 4. (a), (b) and (c).

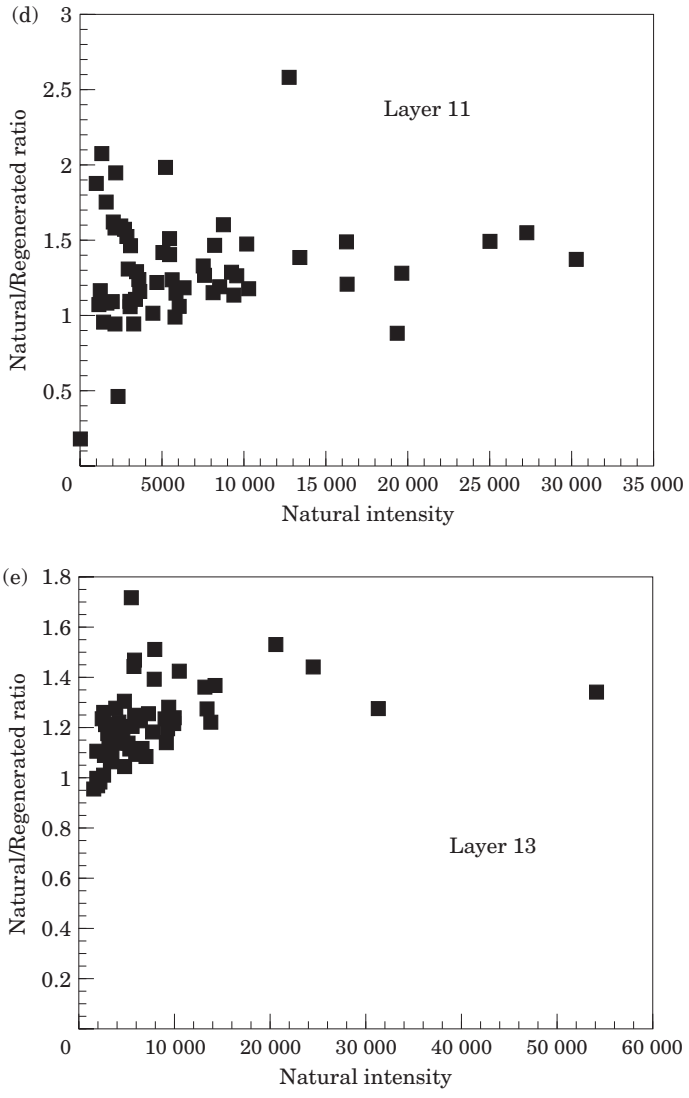

Figure 4. (d) and (e).

Figure 4. The natural signal intensity plotted against the ratios from the previous figure, for each sample. A positive correlation would indicate non-uniform bleaching.

plain). To estimate the dose rate, it was assumed the contribution from the back and sides of the cave was negligible. From the front of the cave, the dose rate from below a zenith angle of about 45° was assumed attenuated by 5·5 m of rock at a relative density of 2·5 plus the sediment overburden (density of 2·0). Above 45° the dose rate was assumed attenuated only by the sediment overburden. The zenith angle takes into consideration the location of the samples about 6 m back of the dripline. Dose rates were calculated according to an angular distribution of cosmic radiation depending on the $\cos^2 \theta$ law (Smith *et al.*, 1997) and by the attenuation formula of

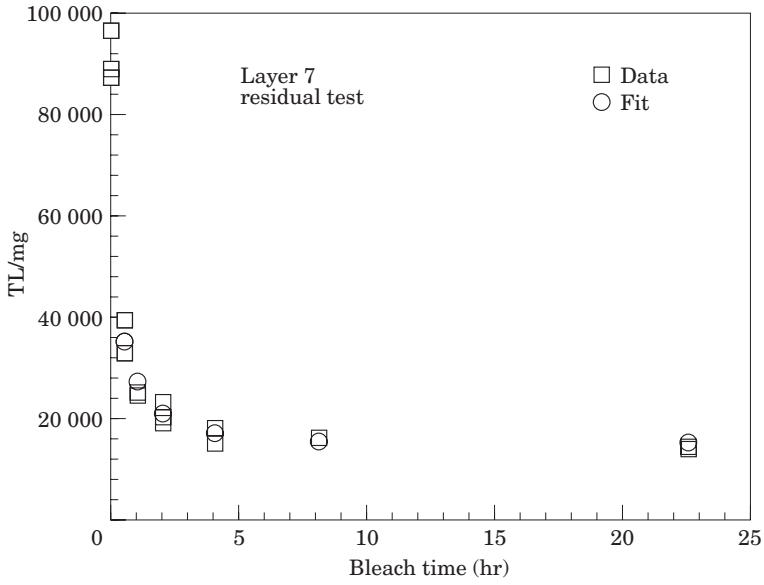

Figure 5. The loss of the TL signals from the slowly bleaching peak of Layer 7 as a function of bleach time. An exponential to all points but the unbleached natural signal provides the fitted values.

Prescott & Hutton (1988). Values are given in Table 3.

A moisture content of 0·026 (ratio of water to dry mass) was derived from the present, rather arid condition of the sediment. This is surely an underestimate of past conditions. Sedimentological and faunal evidence suggests that much of the MSA was deposited during cooler, wetter climate and that the cave may have been a conduit for drainage of ground water during that time (Avery *et al.*, 1997; Tankard & Schweitzer, 1976). In addition, some of the deposits above the MSA may have been deposited in standing water. The porosity of well-sorted sands such as these is estimated to vary between 34–45% on a volume basis (P. Goldberg and G. Salvucci, personal communications; McCuen *et al.*, 1981), which translates to 0·19–0·30 moisture content in terms of mass ratio (assuming the relative density of the dry mass to be about 2·7). Capacity is also affected by compaction, which all these sediments have undergone through time (Tankard & Schweitzer, 1976). Estimating past water contents therefore involves some guesswork. The sediments cannot have been saturated all of the time, not when they were deposited when the cave was periodically occupied and not during at least the last 6000 years when climatic conditions were similar to present. The lower sediments are likely to have had a higher degree of saturation for longer periods of time than upper sediments. Ages were calculated using a moisture content of $0{\cdot}15 \pm 0{\cdot}05$, which should cover most possibilities. How the ages are affected by deviations from this average will be discussed.

Equivalent dose

Preheat

Figure 2 shows the natural/regenerated ratio (of the first 60 s OSL) for several aliquots given different five-minute preheats for the sample from Layer 4/5. Data for OSL signals measured at 30°C and 100°C are given. The 30°C measurements show a plateau in the 210–220°C range, while the

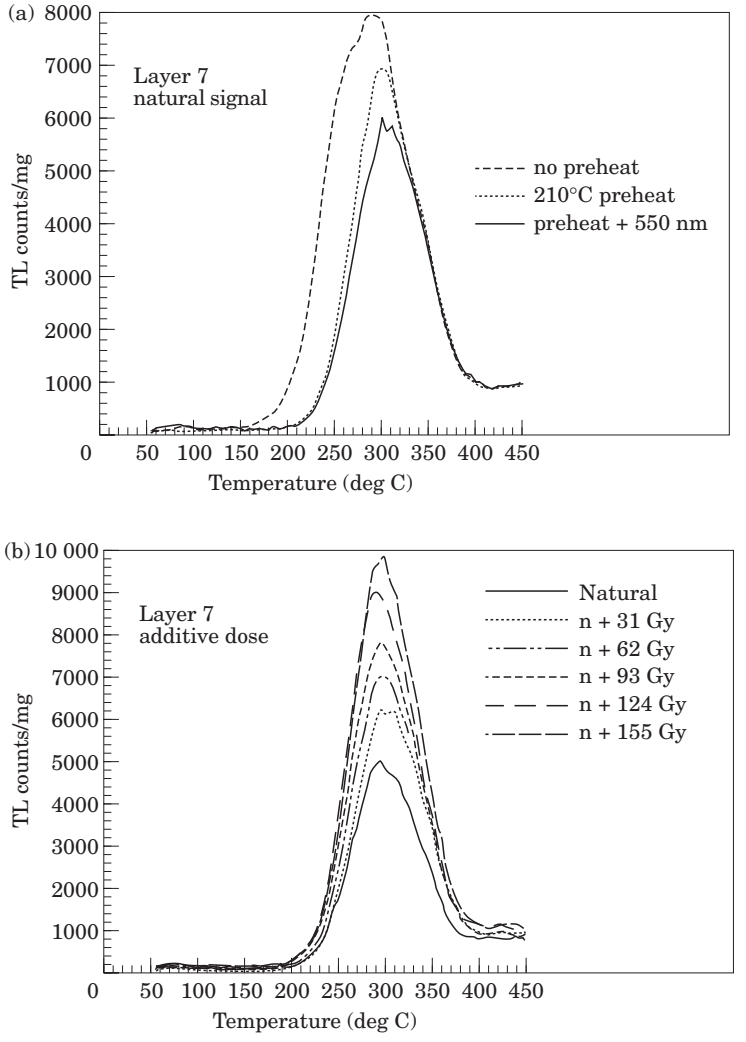

Figure 6 (a) and (b).

100°C measurements show a slightly higher plateau at 220–230°C. Other samples show similar behavior with plateaus generally in the 210–230°C range at both excitation temperatures. Both Layer 7 and Layer 11, for example, showed plateaus covering this range at both temperatures. Subsequent OSL measurements were taken using preheats in this range. A similar test was conducted using IRSL for the Layer 11 sample. A nearly constant ratio from 180–220°C was observed, similar to the plateau reported for feldspars by Duller & Bøtter-Jensen (1993). The declining ratio with preheat evident in the OSL of quartz can be explained by unrealized charge transfer in the irradiated as opposed to the natural material. If a long time period permits transfer from shallow traps to the deep trap responsible for the OSL signal, at low preheats the transfer for the laboratory irradiated material will not be completed, making the regeneration signal

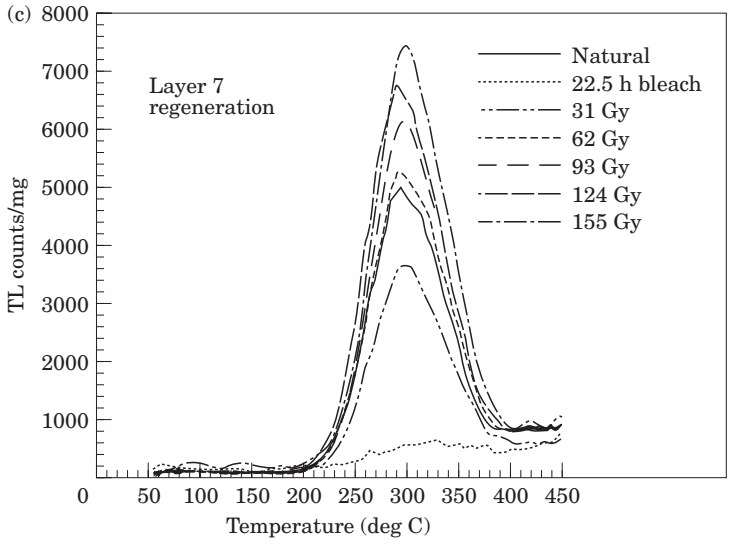

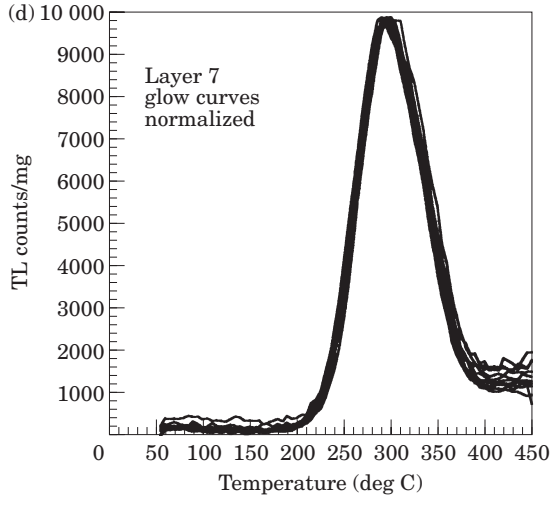

Figure 6. (c) and (d).

Figure 6. (a) The natural signal for the sample from Layer 7 with and without a preheat and after a 30 minute bleach with 550 nm light. After the bleach the remaining signal constitutes the slowly bleaching peak (SBP). (b) Additive dose glow curves for the SBP of the same sample. (c) Regeneration glow curves after a 22·5 h bleach by a solar simulator compared with the natural signal for the same sample. (d) Normalization by peak height of the same glow curves. The region of coincidence (230–370°C) indicates a region of signal stability, or ''plateau''.

smaller (Smith & Rhodes, 1994). Alternatively, if redistribution of charge among luminescence centers over a long time period affects the OSL sensitivity, at low preheats sensitization of the laboratory irradiated material will not be fully realized, making the regeneration signal smaller (Wintle & Murray, 2000).

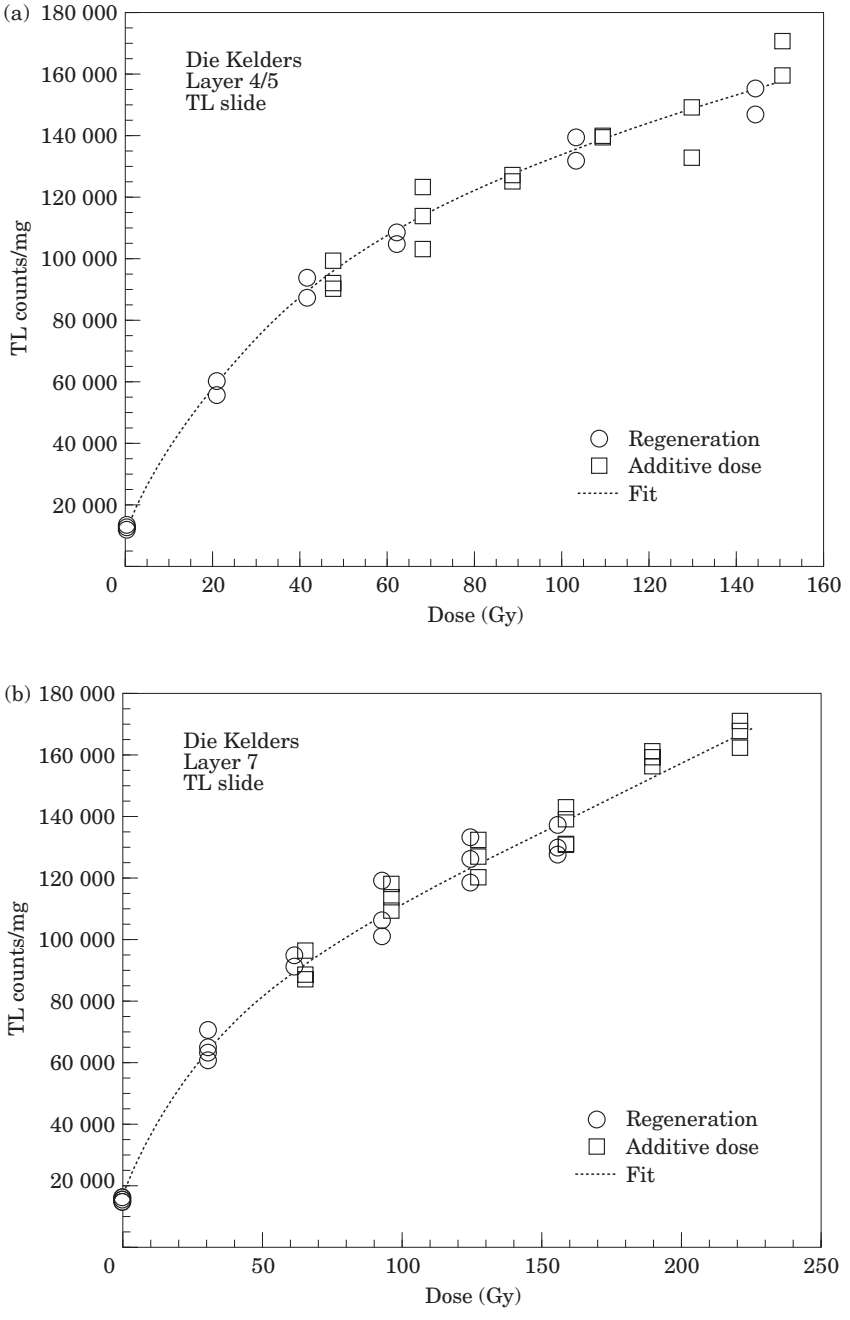

Figure 7. (a) and (b).

Bleaching

Luminescence dating of sediments is valid only if the signal was fully reduced by sunlight at the time of interest or, if a residual signal remains, the residual is determinable. Figure 3 shows histograms of the natural/

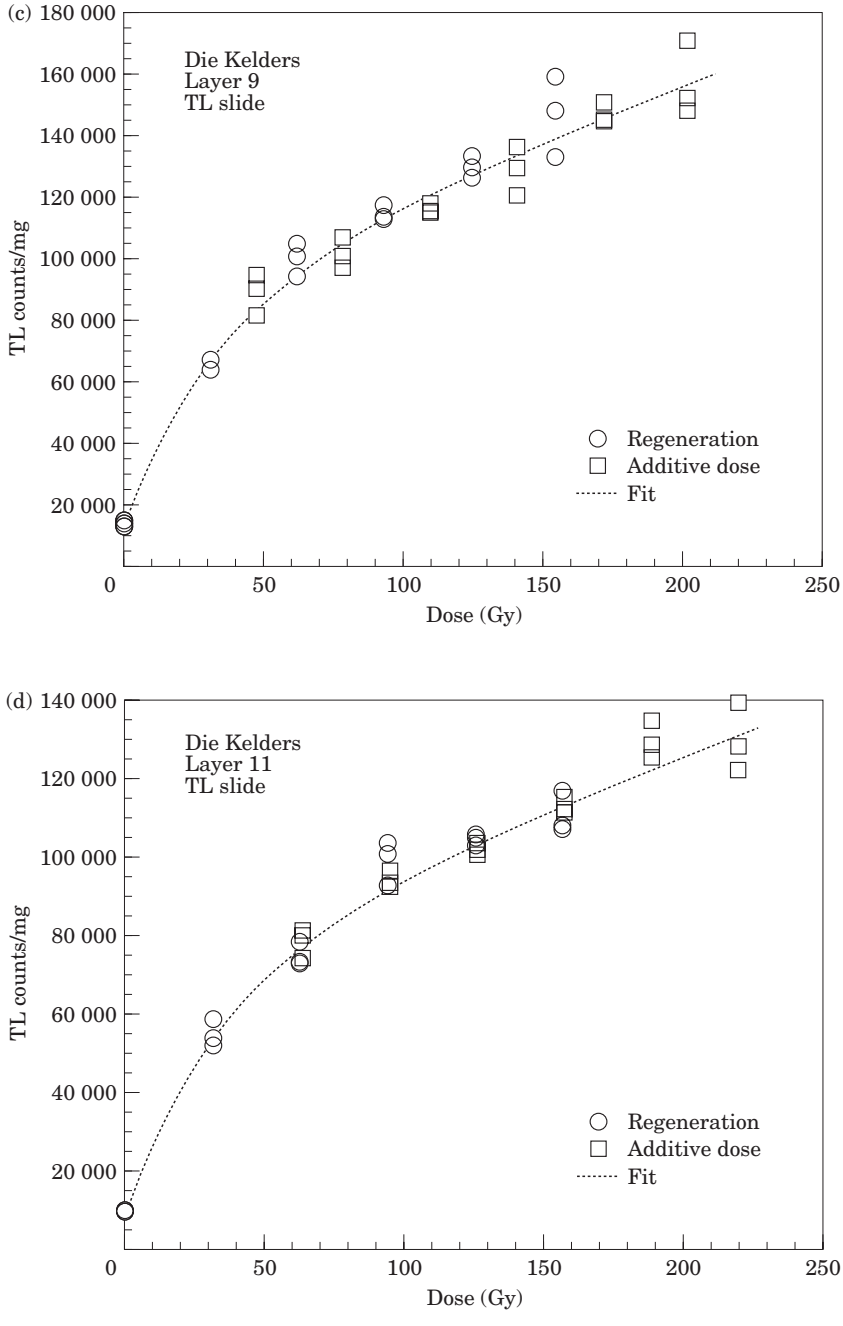

Figure 7. (c) and (d).

regenerated ratios (using the first 60 s of the OSL signal) for the 100-grain aliquots for each sample. The insets show Q-Q (quantile) plots comparing the observed data with those expected in normal distributions. Despite a few outliers, with relatively large

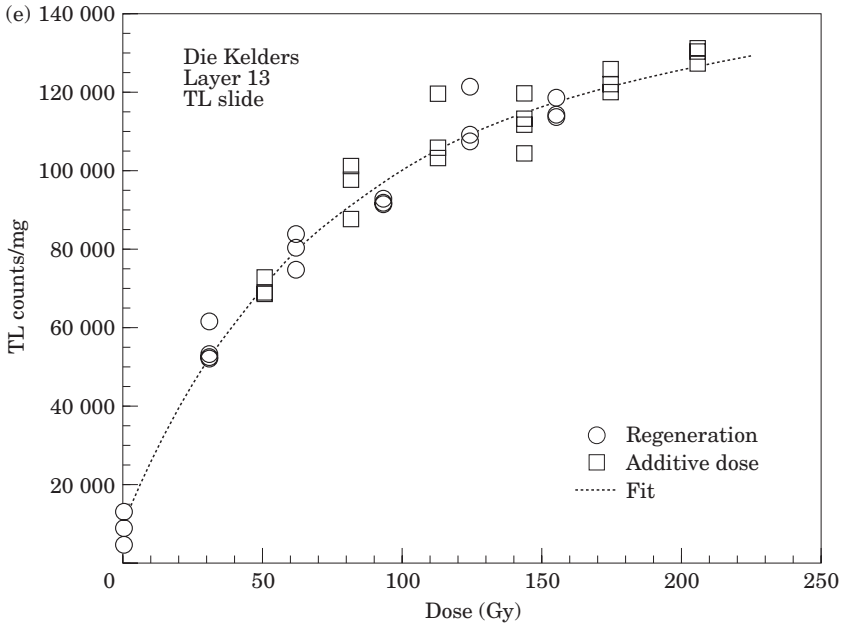

Figure 7. (e).

Figure 7. TL additive dose and regeneration growth curves for each sample, illustrating the ''Australian slide'' method (Huntley *et al.*, 1983*a*). The additive dose points have been shifted horizontally by the same amount to bring them into coincidence with the regenerative points. The fit to both sets of data after the shift are saturating exponentials with linear extensions. The amount of shift provides an estimate for the equivalent dose, which graphically is represented by the position on the dose axis of the lowest additive points (the natural signal). Because of sensitivity change, the shift for samples from Layers 9 and 11 followed a scaling of the regeneration points.

natural signals suggestive of poor bleaching, the bulk of the aliquots cluster tightly around the modal value and form a near normal distribution. To test for normality, a Kolmogorov–Smirnov one-sample test was performed. The K–S z score, a goodness of fit statistic, and the two-tailed probability for a normal distribution is given for each sample in Table 4. At a 95% confidence interval, no sample deviates significantly from normality. The distribution from Layer 11 appears much broader than from the other samples, but still is normal. No other evidence suggested this sample was less well bleached than the others, although it did differ significantly from the others in luminescence sensitivity, somewhat surprisingly given the presumed common source. This may explain the different distribution. At any rate, the broad and skewed distributions reported in the literature for poorly bleached samples (Lamothe & Auclair, 1997; Murray *et al.*, 1995) are not evident for any of these samples. Nor is there any significant tendency for the brightest natural signals to correlate with the highest ratios, as might be expected if high natural signals signified poorly bleached grains (Li, 1994; Clarke, 1996). These data are displayed in Figure 4.

The conclusion drawn from these data is that the samples were well bleached at the time of deposition, as would be expected for aeolian deposits. The few poorly bleached grains, perhaps contributed by decaying roof fall, do not seem numerous enough to

Table 5 Equivalent dose (Gy)

	TL	OSL (single aliquot)	OSL (multi-aliquot)			IRSL
Sample/preheat	210–220°C	210°C	200°C	210°C	220°C	210°C
Layer 4/5	47·0 ± 3·76		64·9 ± 4·02	58·9 ± 3·73	53·8 ± 3·24	
Layer 7	65·0 ± 5·01		67·6 ± 3·94	58·1 ± 5·73	72·1 ± 4·74	
Layer 9	47·5 ± 4·00		75·8 ± 5·29		61·1 ± 4·58	
	73·4 ± 13·9*					
Layer 11	107 ± 0·20	66·1 ± 4·44		67·6 ± 5·80	58·8 ± 4·0	99·1 ± 8·1
	63·0 ± 8·93*					
Layer 13	50·5 ± 5·38	57·5 ± 4·61		60·6 ± 3·42	53·3 ± 3·5	73·3 ± 5·9

*Requires scaling of regeneration points to correct for sensitivity change. For Layer 9 the scale factor was 0·85, for Layer 11 it was 1·21.

Table 6 Equivalent dose from single aliquots

Layer 11		Layer 13	
Additive dose	Regeneration	Additive dose	Regeneration
36·9	45·0	65·7	31·6
66·4	35·9	78·1	35·2
59·1	38·5	62·6	101·2
54·0	36·6	68·0	36·0
65·6	36·5	74·7	36·8
73·4	40·6	39·3	37·4
58·9	36·0	50·8	34·3
57·3	36·0	55·1	32·2
47·7	36·3	49·8	31·0
	42·5	45·3	
			Ave: 34·3 ± 2·5
Ave: 57·1 ± 11·0	Ave: 38·4 ± 3·2	Ave: 58·9 ± 12·9	(excluding 101·2)

affect D_E determinations significantly. The possibility remains that the grains were poorly bleached, but uniformly so. Since the TL data is from a component that bleaches at a much slower rate than that of the OSL, this possibility can be eliminated if the D_E derived from TL matches that from OSL. This is indeed the case.

Thermoluminescence

The slowly bleaching peak (SBP) in TL not only is reduced at a slower rate, it also contains an unbleachable residual that must be determined. This was done by exposing different aliquots of the natural material for progressively longer times to the solar simulator. The resulting loss of signal is shown for the sample from Layer 7 in Figure 5. A saturating exponential was fitted to the inverse of these data and the inverse of the asymptote taken as the unbleachable residual. The same was done for the other samples.

The region of thermal stability used for analysis was determined by normalizing by peak height all glow curves (natural and irradiated) and determining the region of coincidence. A few curves were shifted slightly horizontally to account for differences in thermal lag. Figure 6(a) shows the

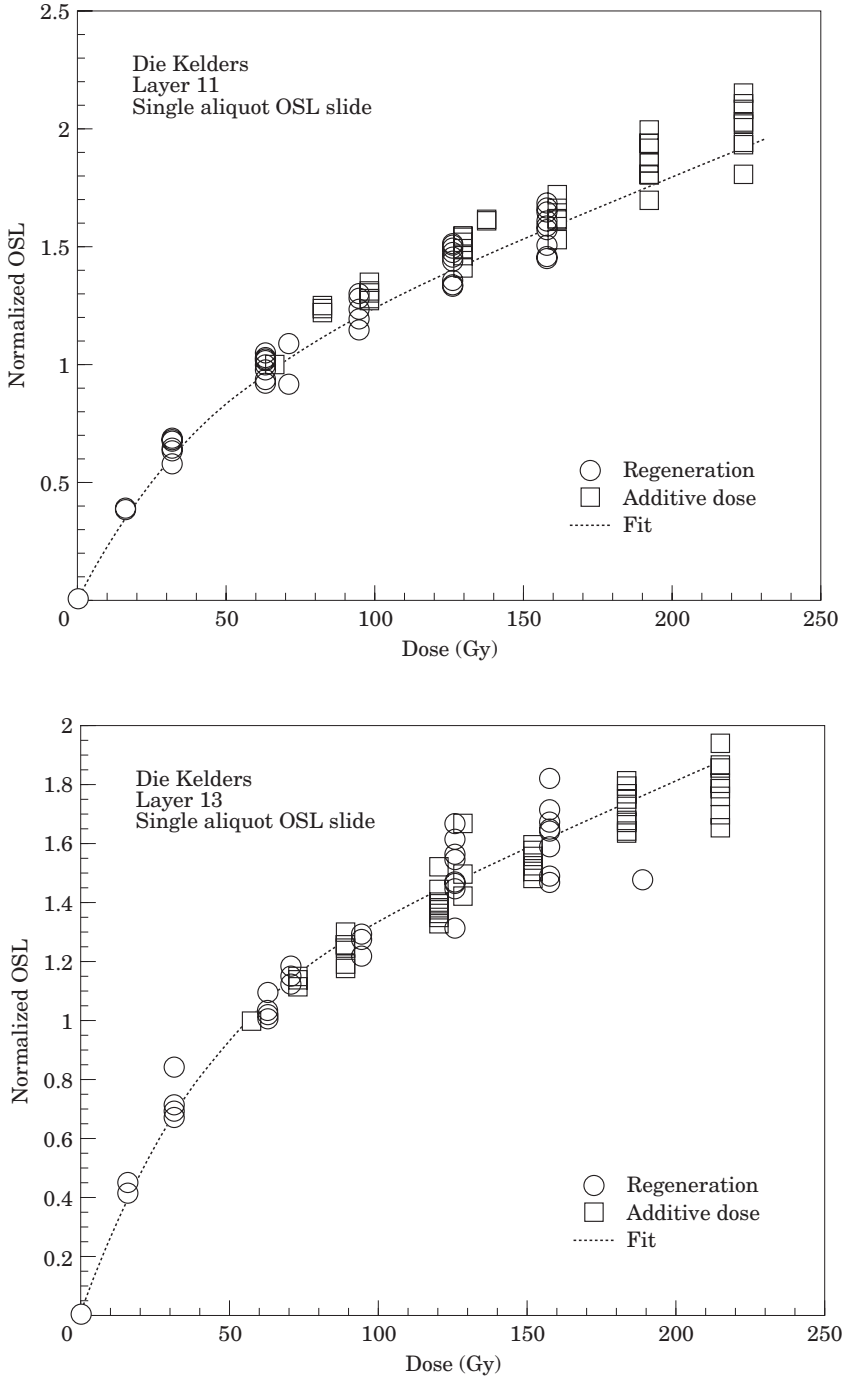

Figure 8. Single aliquot OSL additive dose and regeneration growth curves, normalized by the natural signal and shifted as in Figure 7, for Layers 11 and 13.

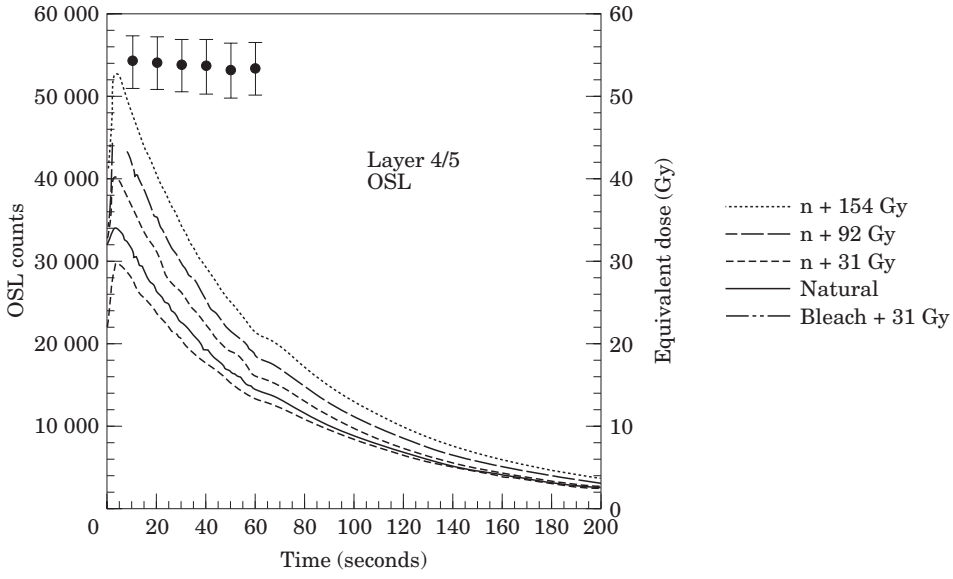

Figure 9. Representative OSL shine down curves in multi-aliquot analysis for the sample from Layer 4/5. The points with error bars represent the equivalent dose calculated for the first six 10 s segments of the shine curve, illustrating a ''time plateau'', where the equivalent dose does not vary with exposure time. (The slight hump after 60 s, noticeable in most of the curves, is an artefact of how the data points were collected. Each data point prior to 60 s represents the signals for one second. After 60 s, each data point represents the average signal for 10 s.)

natural signal for Layer 7, before and after a preheat, and after a 550 nm bleach to produce the SBP. Figure 6(b) and (c) show additive dose and regeneration SBP curves for the same sample. Figure 6(d) shows these same curves normalized to peak height. The stable region for this sample and the others was about 230–370°C, which includes all but the high temperature tail of the SBP.

Figure 7 shows the additive dose and regeneration growth curves for each sample after the additive dose points have been shifted horizontally to coincide with the regeneration points (the ''Australian slide''). The additive dose points for all curves but Layer 4/5 are nearly linear, which may be surprising given the suspected age of these samples. Considering the regeneration curve as well, however, clearly demonstrates that this linearity occurs beyond a sublinear region. The best fit to the combined curves, shown in Figure 7, is a saturating exponential with a linear extension, of the following form (Huntley *et al.*, 1993*a*:7):

$$I = y_o\{1 - \exp[-(D - D_i)/D_o]\} + k(D - D_i)$$

where I is the luminescence intensity, D is the irradiation dose, y_o is the saturation intensity, D_i is the dose intercept, and D_o and k are constants.

Horizontal shifting of the additive dose curve to match the regeneration curve will only succeed if no sensitivity change has occurred from optical zeroing. Sensitivity change, if it is independent of dose, can be corrected with a multiplication, or scale factor, although this is not always recommended if dose dependence cannot be shown (Prescott & Robertson, 1997). For two of the samples (Layer 9 and Layer 11), best fits required scale changes (0·849 for Layer 9 and 1·21 for Layer 11). While the

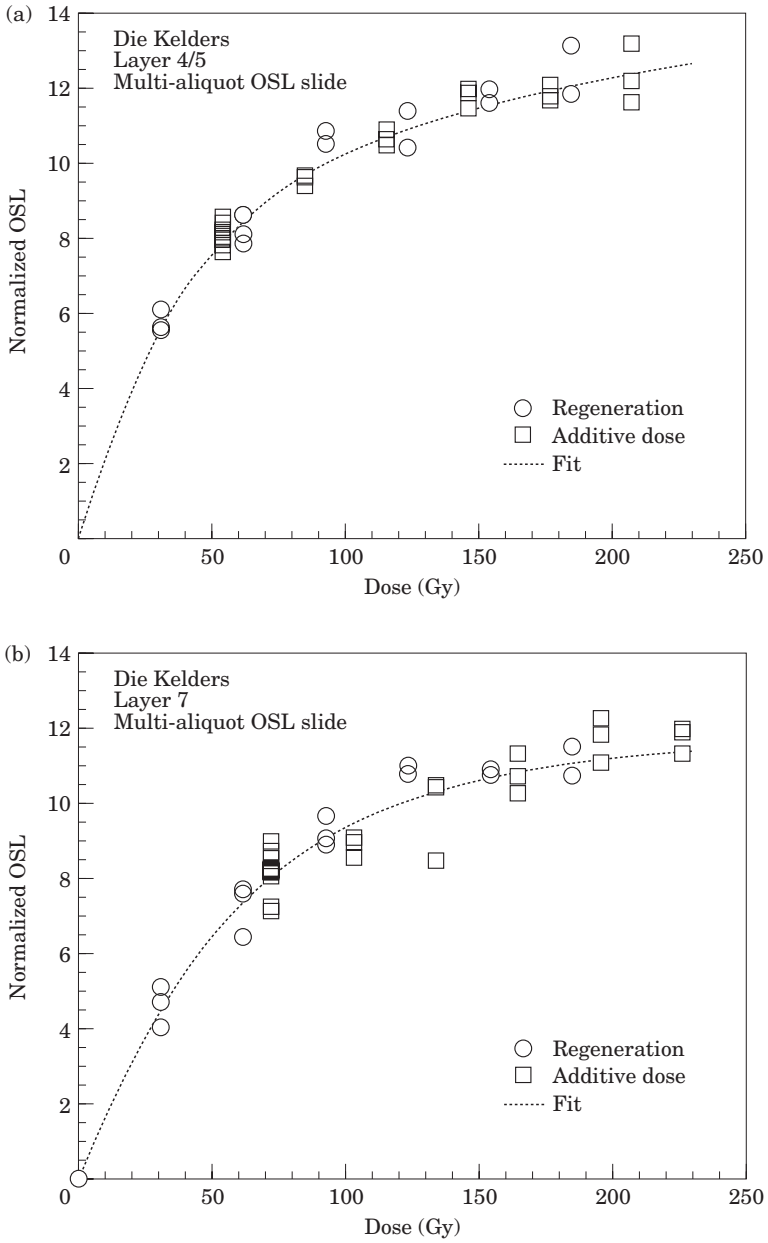

Figure 10. (a) and (b).

legitimacy of correcting for the sensitivity change remains uncertain, the D_Es obtained for these two samples after the scale change agree better with other data than if no scale change had been made. The D_Es, which correspond to the magnitude of shift required to bring the curves into coincidence, are given in Table 5.

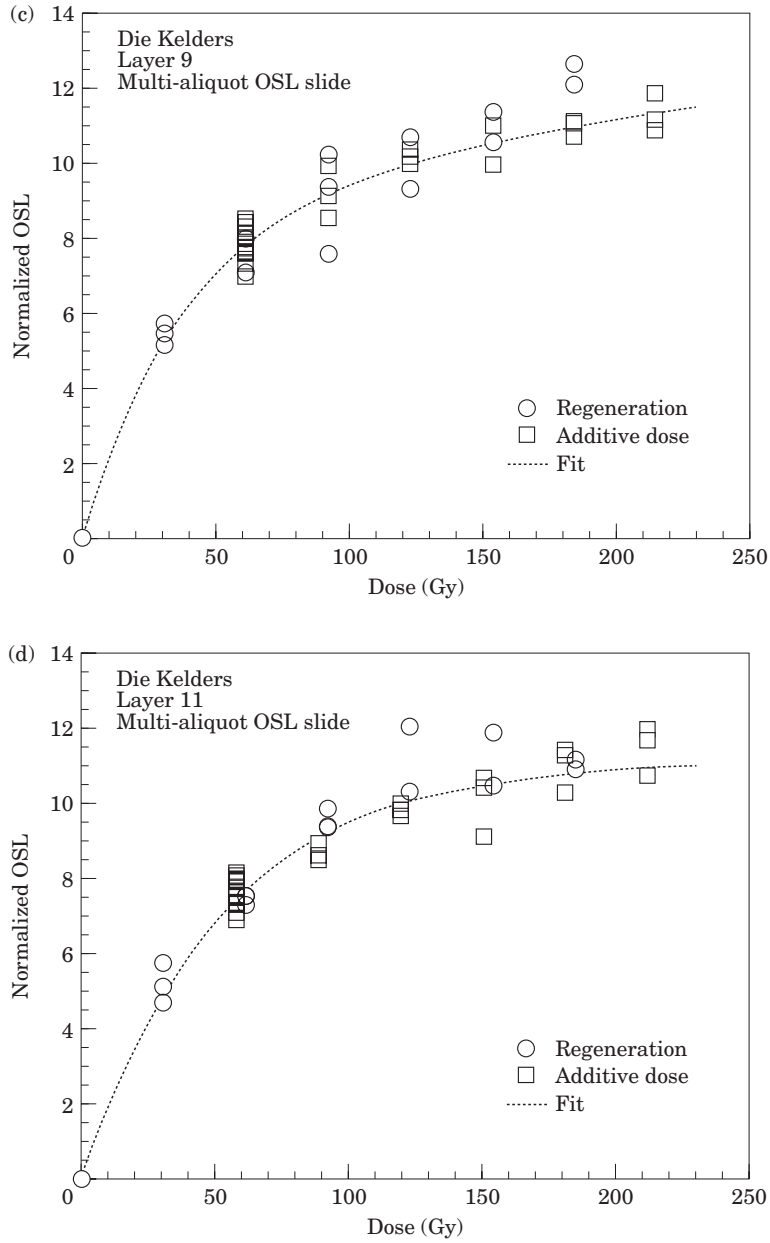

Figure 10. (c) and (d).

Optically stimulated luminescence

OSL signals are often of such magnitude that they can be sampled by repeated short shines without removing a significant amount of the signal. This allows derivation of D_E from single aliquots (Duller, 1995), and because no normalization is required, can sometimes produce better precision.

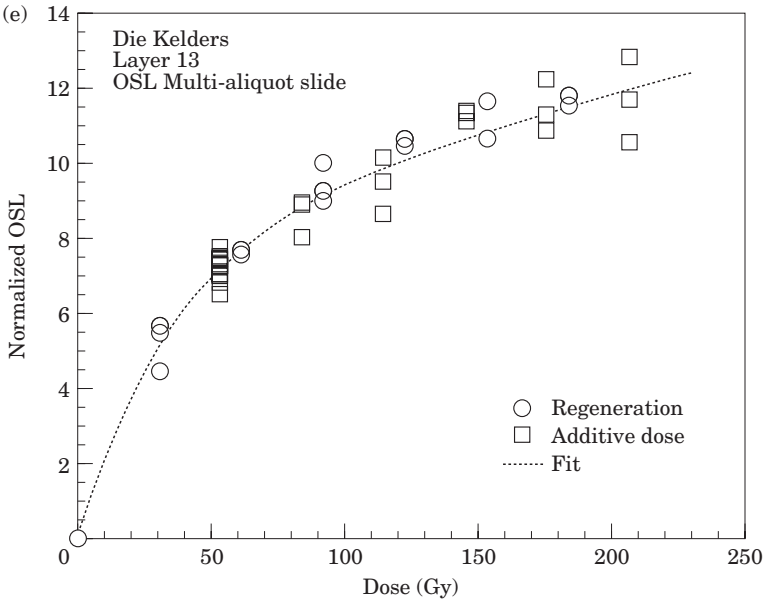

Figure 10. (e).

Figure 10. Multi-aliquot OSL additive dose and regeneration growth curves, shifted as in Figure 7, for each sample.

The procedure involves repeated dosing followed by short (0·1 s) shines to make additive dose or regenerated curves. Because repeated preheats are also necessary, the data must be corrected for loss of signal by the preheats. This can be done by adjusting the luminescence signal by an exponential decay factor determined from successive preheats and shines but without irradiation on the same aliquot after the additive dose or regeneration procedure is completed (Murray *et al.*, 1997). Duller (1994) cautioned that such procedure can cause an underestimation of D_E for saturating curves. Varying the dose increments on different single aliquot analyses can determine whether this problem is significant (Murray *et al.*, 1997). This was done and no difference in results was obtained.

Twenty single aliquot analyses were performed for samples from Layer 11 and Layer 13, using a 210°C 5 min preheat and 0·1 s shines. Results are given in Table 6. The average D_E measured by additive dose differs from that by regeneration. The additive dose D_Es also have a much wider spread of values, which can be attributed to extrapolation errors from the near linearity of the additive dose curves. A more accurate D_E determination should be possible by combining the two sets of measures. This was done by normalizing each single aliquot analysis by its natural signal and combining the data using the ''Australian slide'' technique. This is illustrated in Figure 8 (a few aliquots with markedly different sensitivities than the others were omitted). No sensitivity change between additive dose and regeneration is apparent. The D_E for each sample, taken from the horizontal shift, is given in Table 5. The results agreed with multi-aliquot analyses (presented next) done with a 210°C preheat and improved on precision only slightly for Layer 11 and not at all for Layer 13. Only less time consuming

multi-aliquot analysis was performed for the other samples.

All multi-aliquots were normalized by a 0·1 s shine prior to any measurements. Measurement involved 450 s shines. Only the first 58 s were used for analysis, and the region from 350–390 s was used to subtract background and more difficult to bleach components (Aitken & Xie, 1992). D_Es were initially measured for successive 10 s segments of the shine. For the first 58 s there was no significant difference among the 10 s intervals, so the entire time was integrated. Figure 9 shows some shine curves and the D_Es determined for each 10 s segment for the sample from Layer 4/5, done with a 220°C 5 min preheat. D_E was determined by the slide method, and these data for 220°C 5 min preheats are presented for all samples in Figure 10. No scaling to correct for sensitivity changes was necessary, and the best fits again were saturating exponentials with linear extensions.

Analyses were repeated at different 5 min preheats (from 200° to 220°C). Results where no scaling was necessary are given in Table 5. For four of the samples the D_E decreases with increasing preheat. While a lower D_E is expected for 200°C given the results of the preheat test, the continued decline from 210° to 220°C, although not statistically significant, was not expected at least for some samples, such as Layer 11, where the preheat test showed a plateau in this region. Collection of additional data for the preheat test may possibly demonstrate finer scale differences between 210–220°C. The only exception to the downward trend is for the sample from Layer 7, where a much higher D_E was obtained with a 220°C preheat (again the preheat test showed a plateau from 210°–220°C). This analysis was repeated and similar results obtained. We have no ready explanation for this anomaly and consider the results using the 210°C preheat to be more accurate. For the other four samples we used the results from the 220°C preheat for age calculation.

A potential problem in using preheats for OSL is thermal transfer, where the preheat transfers electrons from thermally stable, light insensitive traps to the trap responsible for the OSL signal, and thereby artificially increases the OSL signal. This was tested for two samples by the following procedure (Huntley *et al.*, 1993*b*). Additive dose and regeneration curves were constructed in the normal way except that after each irradiation (including the natural) and prior to any preheat an 1800 s bleach by the solar simulator was applied. If the preheat transferred charge from a light insensitive trap filled by the irradiation to the OSL trap, then this should register as the only OSL signal by this procedure. This can then be used to correct the OSL signals obtained in the normal way. For both samples, the thermal transferred OSL signal at all doses was less than 1% of the total OSL signal. A correction did not significantly affect the equivalent dose. We conclude that thermal transfer is not a problem for these samples. The difference in OSL signal before and after a preheat for the other samples was similar to the two tested, so thermal transfer was assumed not to be a problem for them either. Use of the slide technique should also minimize any problems with thermal transfer (Rhodes & Bailey, 1997).

Infrared stimulated luminescence

IRSL, characteristic of feldspars, provides an independent determination of the D_E on a different mineral with different luminescence characteristics. Since it was performed on fine grains, it also allows an independent determination on a different grain size. If grains released from disintegrating roof fall have any influence on the age determination, one would not expect agreement in apparent ages from two different grain sizes.

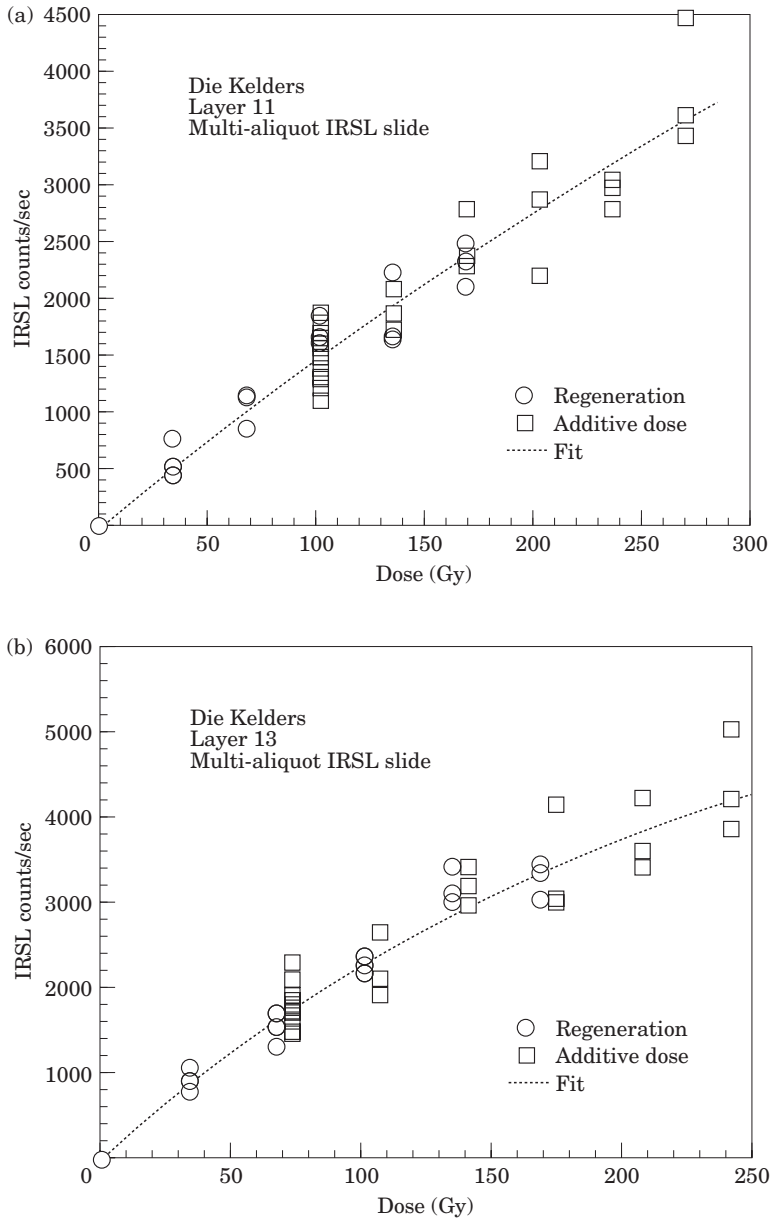

Figure 11. Multi-aliquot IRSL additive dose and regeneration growth curves, shifted as in Figure 7, for Layers 11 and 13.

IRSL was performed only on samples from Layer 11 and Layer 13, using a 5 min preheat at 210°C. Figure 11 shows the fit to the shifted additive dose and regeneration curves. The scatter is high in these curves, largely because normalization by a short shine did not seem to work due to a weak natural signal. The unnormalized data had less scatter. Both curves are nearly linear, although the best fits were saturating

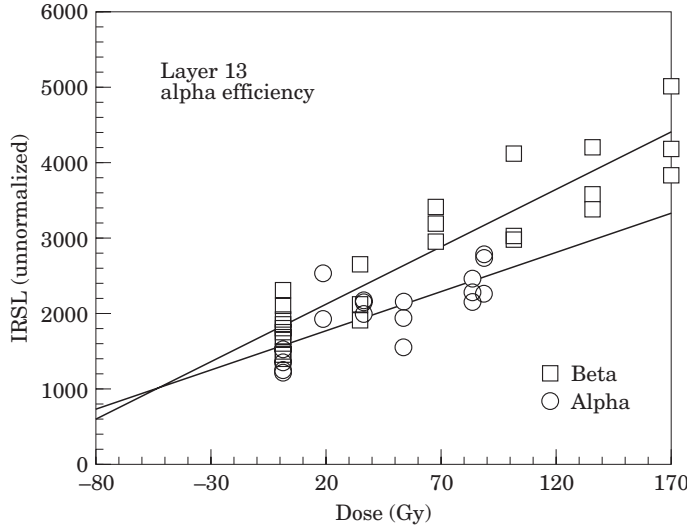

Figure 12. Additive dose curves using beta and alpha irradiation for the sample from Layer 13. The ratio of the slope of these two curves is equivalent to the b-value used to estimate alpha efficiency.

exponentials. As expected, the feldspars, unlike the quartz, were far from saturation. Alpha efficiency was determined by constructing an additive dose curve using alpha irradiation and comparing it with the additive dose using beta (Figure 12). The ratio of slopes produces the ''b-value'', which can be related to alpha efficiency (Aitken, 1985; Lian *et al.*, 1995). A b-value of 0·83–0·09 was obtained. Only the data from Layer 13 are shown. The data from Layer 11 had very high scatter and produced an unreasonable b-value. It was therefore assumed that the b-value for Layer 11 was similar to that of Layer 13.

The D_Es from IRSL are given in Table 5. Feldspars are prone to anomalous fading. Time constraints prevented a direct assessment of any fading, but if the ages from the OSL and IRSL analyses agree, as they do (next section), this would be remarkably coincidental if anomalous fading were a significant factor.

Age calculations

Table 5 shows a near equivalence in D_E for all samples whether determined by TL or OSL (multi or single aliquot). The IRSL results are different because of different grain size and therefore different dose rate. A fuller comparison is given in Table 7, which gives the tabulated ages. The multi-aliquot OSL ages are computed for different moisture contents, as will be discussed shortly. Single-aliquot OSL, TL and IRSL ages are calculated assuming 15% moisture content. There is no significant disagreement between OSL (multi- or single-aliquot), TL or IRSL. The earlier evidence on bleaching demonstrated little grain to grain difference in extent of bleaching, suggesting any contribution of poorly bleached grains from roof fall cannot be significant. The agreement of OSL with TL and IRSL, both of which have different bleaching characteristics than the OSL, affirms this conclusion and also shows that the grains as a whole were not systematically under-bleached. Similar results from independent methods suggest few other systematic problems in D_E determination.

Comparison among the samples shows similar ages for all the samples but a clear stratigraphic inversion. The lower two

Table 7 Derived ages (ka) by technique

	TL	OSL (single aliquot)	OSL (multi-aliquot)				IRSL
Sample/moisture	15%	15%	10%	15%	20%	25%	15%
Layer 4/5	50·7 ± 4·7		55·0 ± 4·3	58·0 ± 4·5	61·0 ± 4·6	63·9 ± 4·8	
Layer 7	75·3 ± 6·8		63·9 ± 7·0	67·3 ± 7·4	70·7 ± 7·7	74·2 ± 8·1	
Layer 9	79·7 ± 15·6		63·0 ± 5·7	66·4 ± 5·9	69·7 ± 6·2	73·1 ± 6·5	
Layer 11	67·0 ± 10	70·3 ± 5·8	59·4 ± 5·0	62·6 ± 5·3	66·7 ± 5·5	68·9 ± 5·7	69·9 ± 6·5
Layer 13	51·4 ± 6·0	58·6 ± 5·4	51·5 ± 4·2	54·3 ± 4·4	57·0 ± 4·5	59·8 ± 4·7	50·6 ± 4·6

samples appear younger than higher samples, although only Layer 13 is significantly younger. Given the lack of evidence for systematic error in the D_E, the most likely source of error is in the dose rate, particularly in accounting for moisture content. The lower samples, particularly the very lowest, are likely to have been wetter for longer periods of time. In Table 7, the ages are recalculated assuming different average moisture contents. If the higher samples were relatively dryer and the lower one wetter, the stratigraphic problems are reduced, although not eliminated.

The best conclusion from these data is that the ages of all five samples are similar and that the differences reflect to some degree uncertainties in the dose rate, particularly in regard to moisture contents. This means that the deposition of the MSA layers occurred over a relatively short time, about 60–70,000 years ago. This agrees in broad terms with the ESR dates, assuming the early uptake model, reported in Avery *et al.* (1997). Sedimentary data suggest deposition during a marine regression. The results reported here place this during the early part of the Late Glaciation as argued by Tankard & Schweitzer (1976) rather than during a cold phase of the Late Interglaciation as argued by Hendey & Volman (1986). While a classic Howieson's Poort assemblage is not present at Die Kelders, the presence of some backed pieces in the upper MSA deposits and the relatively high frequency of cryptocrystalline silcretes in some occupation layers suggest a possible historic affinity. The Howieson's Poort is not well-dated (Parkington, 1990), but evidence from Klasies River Mouth (Deacon *et al.*, 1988; Grun *et al.*, 1990) and Boomplaas Cave (Deacon, 1983) suggest an age of 60–70 ka, in agreement with the dates provided here.

Summary

Five luminescence dates have been obtained from MSA deposits at Die Kelders. The dates are quite similar and average about 60–70 ka, depending in part on assumptions of past moisture content. They agree in general with reported ESR dates. The samples appear to be well bleached, and D_E determined in varied ways produced similar results. The radioactivity in the deposits appears to be generally uniform and shows no evidence of having changed in the past. The dates place the MSA occupations during the early part of the Last Glaciation, in agreement with sedimentary data. The occupations also appear to be congruent in age with Howieson's Poort assemblages elsewhere in South Africa.

Acknowledgements

Collection of samples at Die Kelders was made possible by a grant from the Louis S. B. Leakey Foundation. Laboratory

work was funded by the National Science Foundation grants SBR96-01302 and SBR97-05320 to Feathers. Kris Wilhelmsen assisted with sample preparation. The discussion on moisture content benefited from input by Paul Goldberg and G. Salvucci of Boston University. Constructive criticism of an earlier version by three anonymous reviewers led to some additional data collection and a much improved product.

References

Aitken, M. J. (1985). *Thermoluminescence Dating*. London: Academic Press.

Aitken, M. J. & Xie, J. (1992). Optical dating using infrared diodes: young samples. *Quat. Sci. Rev.* **11,** 147–152.

Avery, G., Cruz-Uribe, K., Goldberg, P., Grine, F. E., Klein, R. G., Lenardi, M. J., Marean, C. W., Rink, W. J., Schwarcz, H. P., Thackeray, A. I. & Wilson, M. L. (1997). The 1992–1993 excavations at the Die Kelders Middle and Later Stone Age cave site, South Africa. *J. Field Arch.* **24,** 263–291.

Bortolot, V. J. (1997). Improved OSL excitation with fiberoptics and focused lamps. *Radiation Meas.* **27,** 101–106.

Brooks, A. S., Cramer, J. S., Franklin, A. D., De Heinzelin, J., Helgren, D. M., Hornyak, W. F., Keating, J. M., Klein, R. G., Schwarcz, H., Leith Smith, J. N., Stewart, K., Todd, N., Verniers, J. & Yellen, J. (1995). Dating and context of three Middle Stone Age sites with bone points in the Upper Semliki Valley, Zaire. *Science* **268,** 548–553.

Butzer, K. W. (1979). Preliminary notes on the geology of Die Kelders Cave, Cape. *Ann. S. Afr. Mus.* **5,** 225–228.

Clarke, M. L. (1996). IRSL dating of sands: bleaching characteristics at deposition inferred from the use of single aliquots. *Radiation Meas.* **26,** 611–620.

Deacon, H. J. (1983). Late Quaternary Environment and Cultural Relationships in the Southern Cape. Report to the Human Sciences Research Council, Department of Anthropology, University of Stellenbosch.

Deacon, H. J., Talma, A. S. & Vogel, J. C. (1988). Biological and cultural development of Pleistocene people in an Old World southern continent. In (J. R. Prescott, Ed.) *Archaeometry: Australasian Studies 1988*, pp. S23–S31. Adelaide: The University of Adelaide.

Duller, G. A. T. (1994). Luminescence dating of sediments using single aliquots: new procedures. *Quat. Sci. Rev.* **13,** 149–156.

Duller, G. A. T. (1995). Luminescence dating using single aliquots: methods and applications. *Radiation Meas.* **24,** 217–226.

Duller, G. A. T. & Bøtter-Jensen, L. (1993). Luminescence from potassium feldspars stimulated by infrared and green light. *Radiation Protection Dosimetry* **47,** 683–688.

Feathers, J. K. (1997). Luminescence dating of sediment samples from White Paintings Rockshelter, Botswana. *Quat. Geochron.* **16,** 321–331.

Franklin, A. D. & Hornyak, W. F. (1990). Isolation of the rapidly bleaching peak in quartz TL glow curves. *Ancient TL* **8,** 29–31.

Grine, F. E., Klein, R. G. & Volman, T. P. (1991). Dating archaeological and human fossils from theMiddle Stone Age levels of Die Kelders, South Africa. *J. hum. Evol.* **21,** 363–395.

Grün, R., Shackleton, N. J. & Deacon, H. J. (1990). Electron-spin-resonance dating of tooth enamel from Klasies River Mouth cave. *Curr. Anthrop.* **31,** 427–432.

Grün, R., Brink, J. S., Spooner, N. A., Taylor, L., Stringer, C. B., Franciscus, R. G. & Murray, A. S. (1996). Direct dating of Florisbad hominid. *Nature* **382,** 500–501.

Hendey, Q. B. & Volman, T. P. (1986). Last interglacial sea levels and coastal caves in the Cape Province, South Africa. *Quat. Res.* **25,** 189–198.

Huntley, D. J., Hutton, J. T. & Prescott, J. R. (1993*a*). The stranded beach-dune sequence of south-east South Australia: a test of thermoluminescence dating, 0–800 ka. *Quat. Sci. Rev.* **12,** 1–20.

Huntley, D. J., Hutton, J. T. & Prescott, J. R. (1993*b*). Optical dating using inclusions within quartz grains. *Geology* **21,** 1087–1090.

Lamothe, M. & Auclair, M. (1997). Assessing the datability of young sediments by IRSL using an intrinsic laboratory protocol. *Radiation Meas.* **27,** 107–117.

Li, S.-H. (1994). Optical dating: insufficiently bleached sediments. *Radiation Meas.* **23,** 563–567.

Lian, O. B., Hu, J., Huntley, D. J. & Hicock, S. R. (1995). Optical dating studies of Quaternary organic-rich sediments from southwestern British Columbia and northwestern Washington State. *Can. J. Earth Sci.* **32,** 1194–1207.

McCuen, R. H., Rawls, W. J. & Brakensiek, D. L. (1981). Statistical analysis of the Brooks-Corey and Green-Ampt parameters across soil textures. *Water Resources Research* **17,** 1005–1013.

Murray, A. S., Marten, R., Johnston, A. & Martin, P. (1987). Analysis for naturally occurring radionuclides at environmental concentrations by gamma spectrometry. *J. Radioanal. Nucl. Chem.* **115,** 263–288.

Murray, A. S., Olley, J. M. & Caitcheon, G. G. (1995). Measurement of equivalent doses in quartz from contemporary water-lain sediments using optically stimulated luminescence. *Quat. Sci. Rev.* **14,** 365–371.

Murray, A. S., Roberts, R. G. & Wintle, A. G. (1997). Equivalent dose measurement using a single aliquot of quartz. *Radiation Meas.* **27,** 171–184.

Nambi, K. S. V. & Aitken, M. J. (1986). Annual-dose conversion factors for TL and ESR dating. *Archaeometry* **28,** 202–205.

Parkington, J. (1990). A critique of the consensus view on the age of Howieson's Poort assemblages in South Africa. In (P. Mellars, Ed.) *The Emergence of Modern Humans*, pp. 34–55. Edinburgh: Edinburgh University Press.

Prescott, J. R. & Hutton, J. T. (1988). Cosmic ray and gamma ray dosimetry for TL and ESR. *Nucl. Tracks Radiation Meas.* **14,** 223–227.

Prescott, J. R. & Robertson, G. B. (1997). Sediment dating by luminescence: a review. *Radiation Meas.* **27,** 893–922.

Rhodes, E. J. & Bailey, R. M. (1997). The effect of thermal transfer on the zeroing of the luminescence of quartz from recent glaciofluvial sediments. *Quat. Sci. Rev.* **16,** 291–298.

Roberts, R., Bird, M., Olley, J., Galbraith, R., Lawson, E., Laslett, G., Yoshida, H., Jones, R., Fullagar, R., Jacobsen, G. & Hua, Q. (1998). Optical and radiocarbon dating at Jinmium rock shelter in northern Australia. *Nature* **393,** 358–362.

Smith, B. W. & Rhodes, E. J. (1994). Charge movements in quartz and their relevance to optical dating. *Radiation Meas.* **23,** 329–333.

Smith, M. A., Prescott, J. R. & Head, M. J. (1997). Comparison of ^{14}C and luminescence chronologies at Puritjarra Rock Shelter, Central Australia. *Quat. Geochron.* **16,** 299–320.

Tankard, A. J. & Schweitzer, F. R. (1974). The geology of Die Kelders Cave and environs: a palaeoenvironmental study. *S. Afr. J. Sci.* **70,** 365–369.

Tankard, A. J. & Schweitzer, F. R. (1976). Textural analysis of cave sediments: Die Kelders, Cape Province, South Africa. In (D. A. Davidson & M. L. Shackley, Eds) *Geoarchaeology*, pp. 289–316. London: Duckworth.

Wintle, A. G. & Murray, A. S. (2000). Towards the development of a preheat procedure for OSL dating of quartz. *Radiation Meas.* (in press).